

# A PROGRESSIVE REFINEMENT APPROACH FOR THE VISUALISATION OF IMPLICIT SURFACES

Manuel N. Gamito\*

*Department of Computer Science  
The University of Sheffield  
M.Gamito@dcs.shef.ac.uk*

Steve C. Maddock

*Department of Computer Science  
The University of Sheffield  
S.Maddock@dcs.shef.ac.uk*

Keywords: Affine arithmetic, implicit surface, progressive refinement, ray casting.

Abstract: Visualising implicit surfaces with the ray casting method is a slow procedure. The design cycle of a new implicit surface is, therefore, fraught with long latency times as a user must wait for the surface to be rendered before being able to decide what changes should be introduced in the next iteration. In this paper, we present an attempt at reducing the design cycle of an implicit surface modeler by introducing a progressive refinement rendering approach to the visualisation of implicit surfaces. This progressive refinement renderer provides a quick previewing facility. It first displays a low quality estimate of what the final rendering is going to be and, as the computation progresses, increases the quality of this estimate at a steady rate. The progressive refinement algorithm is based on the adaptive subdivision of the viewing frustum into smaller cells. An estimate for the variation of the implicit function inside each cell is obtained with an affine arithmetic range estimation technique. Overall, we show that our progressive refinement approach not only provides the user with visual feedback as the rendering advances but is also capable of completing the image faster than a conventional implicit surface rendering algorithm based on ray casting.

## 1 INTRODUCTION

Implicit surfaces play an important role in Computer Graphics. Surfaces exhibiting complex topologies, i.e. with many holes or disconnected pieces, can be easily modelled in implicit form (Desbrun and Gascuel, 1995; Whitaker, 1998; Foster and Fedkiw, 2001). An implicit surface is defined as the set of all points  $\mathbf{x}$  that verify the condition  $f(\mathbf{x}) = 0$  for some function  $f(\mathbf{x})$  from  $\mathbb{R}^3$  to  $\mathbb{R}$ . Modelling with implicit surfaces amounts to the construction of an appropriate function  $f(\mathbf{x})$  that will generate the desired surface.

Rendering algorithms for implicit surfaces can be broadly divided into meshing algorithms and ray casting algorithms. Meshing algorithms convert an implicit surface to a polygonal mesh format, which can be subsequently rendered in real time with modern graphics processor boards (Lorensen and Cline, 1987; Bloomenthal, 1988; Velho, 1996). Ray casting algorithms bypass mesh generation entirely and compute instead the projection of an implicit surface on the screen by casting rays from each pixel into

three-dimensional space and finding their intersection with the surface (Roth, 1982; Hin et al., 1989).

Our ultimate goal is to use implicit surfaces as a tool to model and visualise realistic procedural planets over a very wide range of scales. The function  $f(\mathbf{x})$  that generates the surface terrain for such a planet must have fractal scaling properties and exhibit a large amount of small scale detail. Examples of this type of terrain generating function can be found in the Computer Graphics literature (Ebert et al., 2003). In our planet modelling scenario, meshing algorithms are too cumbersome as they generate meshes with a very high polygon count in order to preserve all the visible surface detail. Furthermore, as the viewing distance changes, the amount of surface detail varies accordingly and the whole polygon mesh needs to be regenerated. For these reasons, we have preferred a ray casting approach because of its ability to render the surface directly without the need for an intermediate polygonal representation.

The visualisation of an implicit surface with ray casting is not without its problems, however. When the surface is complex, many iterations have to be performed along each ray in order to locate the intersection point with an acceptable accuracy (Mitchell,

---

\*Supported by grant SFRH/BD/16249/2004 from Fundação para a Ciência e a Tecnologia, Portugal.

1990). Imaging an implicit surface with ray casting can then become a slow procedure. This is further compounded by the fact that an anti-aliased image requires that many rays be shot for each pixel (Cook, 1989).

We propose to alleviate the long rendering times associated with the modelling and subsequent ray casting of complex fractal surfaces by providing a quick previewer based on a progressive refinement rendering principle. The idea of progressive refinement for image rendering was first formalised in 1986 (Bergman et al., 1986). Progressive refinement rendering has received much attention in the fields of radiosity and global illumination (Cohen et al., 1988; Guo, 1998; Farrugia and Peroche, 2004). Progressive refinement approaches to volume rendering have also been developed (Laur and Hanrahan, 1991; Lippert and Gross, 1995). Our previewer uses progressive rendering to visualise an increasingly better approximation to the final implicit surface. It allows the user to make quick editing decisions without having to wait for a full ray casting solution to be computed. Because the rendering is progressive, the previewer can be terminated as soon as the user is satisfied or not with the look of the surface. The previewer is also capable of completing the image in a shorter amount of time than it would take for a ray caster to render the same image by shooting a single ray through the centre of each pixel.

## 2 RENDERING WITH PROGRESSIVE REFINEMENT

The main stage of our method consists in the binary subdivision of the space, visible from the camera, into progressively smaller cells that are known to straddle the boundary of the surface. The subdivision mechanism stops as soon as the projected size of a cell on the screen becomes smaller than the size of a pixel. Information about the behaviour of the implicit function  $f(\mathbf{x})$  inside a cell is returned by evaluating the function with affine arithmetic (Comba and Stolfi, 1993). Affine arithmetic is a framework for evaluating algebraic functions with arguments that are bounded but otherwise unknown. It is a generalisation of the older interval arithmetic framework (Moore, 1966). Affine arithmetic, when compared against interval arithmetic, is capable of returning much tighter estimates for the variation of a function, given input arguments that vary over the same given range. Affine arithmetic has been used with success in an increasing number of Computer Graphics problems, including the ray casting of implicit surfaces (Heidrich and Seidel, 1998; Heidrich et al., 1998; de Figueiredo, 1996; Junior et al., 1999; de Figueiredo et al., 2003). We use

a simpler form of affine arithmetic known as *Affine Form 1* (AF1), which we term *reduced affine arithmetic* (Messine, 2002). Reduced affine arithmetic, in the context of ray casting implicit surfaces made from procedural fractal functions, returns the same results as standard affine arithmetic while being faster to compute and requiring smaller data structures.

The procedure for rendering implicit surfaces with progressive refinement can be broken down into the following steps:

1. Build an initial cell coincident with the camera's viewing frustum. The near and far clipping planes are determined so as to bound the implicit surface.
2. Recursively subdivide this cell into smaller cells. Discard cells that do not intersect with the implicit surface. Stop subdivision if the size of the cell's projection on the image plane falls below the size of a pixel.
3. Assign the shading value of a cell to all pixels that are contained inside its projection on the image plane. The shading value for a cell is taken from the evaluation of the shading model at the centre point of the cell.

The Rayshade public domain ray tracer implements a previewing tool that traces rays at the corners of rectangular regions in the image and subdivides these regions based on their estimated contrast (Kolb, 1992). Since the ray casting of implicit surfaces is one instance of the more general ray tracing problem, the same previewing mechanism could be used here. In a ray tracer, the process of ray-surface intersection is performed independently for each ray, with no information being shared between neighbouring rays. When a cell is subdivided, on the other hand, the information about the implicit surface contained in that cell is refined and passed down to the child cells. A previewer for implicit surfaces that uses cell subdivision will, therefore, converge more quickly than a generic previewer that uses subdivision in image space, as implemented in Rayshade.

Another previewing method for implicit surfaces with some similarities to ours was briefly described as part of a larger work (de Figueiredo and Stolfi, 1996). A subdivision of space using an octree is proposed to track the boundary of the surface with increasing accuracy. Surface visibility is determined by a painter's algorithm whereby the octree is traversed in back to front order, relative to the camera, as the cells are rendered on the screen. Our method is more efficient and less memory intensive in that only the cells that are known to be visible from the camera are considered. No time is wasted tracking and subdividing cells that lie on hidden portions of the surface. The following sections will explain how each of the steps in our rendering method work.

## 2.1 Reduced Affine Arithmetic

A variable is represented with reduced affine arithmetic (rAA) as a central value plus a series of noise symbols. In contrast to the standard affine arithmetic model, the number of noise symbols is constant and can be used to describe the fundamental degrees of freedom of the problem under consideration (Messine, 2002). In the rendering method that is being described in this paper, the degrees of freedom are the three parameters necessary to locate any point inside the viewing frustum of the camera. These parameters are the horizontal distance  $u$  along the image plane, the vertical distance  $v$  along the same image plane and the distance  $t$  along the ray that passes through the point at  $(u, v)$ . A rAA variable  $\hat{a}$  has, therefore, the following representation:

$$\hat{a} = a_0 + a_u e_u + a_v e_v + a_t e_t + a_k e_k. \quad (1)$$

The extra noise symbol  $e_k$  is included to account for uncertainties in the  $\hat{a}$  variable that are not shared with any other variable. Operations on rAA variables are performed by updating the  $a_u$ ,  $a_v$  and  $a_t$  noise coefficients with new uncertainties related to the  $u$ ,  $v$  and  $t$  view frustum distances and clumping all other uncertainties into the  $a_k$  coefficient.

For an implicit surface, the vector  $\mathbf{x}$  at some point in space can be described in rAA format as a tuple of three cartesian coordinates, with the representation in (1), and where the noise symbols  $e_u$ ,  $e_v$  and  $e_t$  are shared between the coordinates. Each coordinate has its own independent noise symbol  $e_{k_i}$ , with  $i = 1, 2, 3$ . The rAA representation  $\hat{\mathbf{x}}$  of the vector  $\mathbf{x}$  describes not a point but a region of space spanned by the uncertainties associated with its three coordinates. Evaluation of the expression  $\hat{y} = f(\hat{\mathbf{x}})$  leads to a range estimate  $\hat{y}$  for the variation of  $f(\hat{\mathbf{x}})$  inside the region spanned by  $\hat{\mathbf{x}}$ . Knowing  $\hat{y}$ , the average value  $\bar{y}$  and the variance  $\langle y \rangle$  for that range estimate can be computed as follows, based on the representation in (1) for an rAA variable:

$$\bar{y} \triangleq y_0, \quad (2a)$$

$$\langle y \rangle \triangleq |y_u| + |y_v| + |y_t| + |y_k|. \quad (2b)$$

The range estimate  $\hat{y}$  is then known to lie inside the interval  $[\bar{y} - \langle y \rangle, \bar{y} + \langle y \rangle]$ . If this interval contains zero, the region spanned by  $\hat{\mathbf{x}}$  may or may not intersect with the implicit function. This is because affine arithmetic (both in its standard and reduced forms) always computes conservative range estimates and it is possible that the exact range resulting from  $f(\hat{\mathbf{x}})$  may be smaller than  $\hat{y}$ . What is certain is that if  $[\bar{y} - \langle y \rangle, \bar{y} + \langle y \rangle]$  does not contain zero the region spanned by  $\hat{\mathbf{x}}$  is either completely inside or completely outside the implicit surface and therefore does not intersect it.

## 2.2 The Anatomy of a Cell

A cell is a portion of the camera's viewing frustum that results from a recursive subdivision along the  $u$ ,  $v$  and  $t$  parameters. Figure 1 depicts the geometry of a cell. It has the shape of a truncated pyramid of quadrangular cross-section, similar to the shape of the viewing frustum itself. Four vectors, taken from the camera's viewing system, are used to define the spatial extent of a cell. These vectors are:

**The vector  $\mathbf{o}$**  This is the location of the camera in the world coordinate system.

**The vectors  $\mathbf{p}_u$  and  $\mathbf{p}_v$**  They represent the horizontal and vertical direction along the image plane. The length of these vectors gives the width and height, respectively, of a pixel in the image plane.

**The vector  $\mathbf{p}_t$**  It is the vector from the camera's viewpoint and orthogonal to the image plane. The length of this vector gives the distance from the viewpoint to the image plane.

The vectors  $\mathbf{p}_u$ ,  $\mathbf{p}_v$  and  $\mathbf{p}_t$  define a left-handed perspective viewing system. The position of any point  $\mathbf{x}$  inside the cell is given by the following inverse perspective transformation:

$$\begin{aligned} \mathbf{x} &= \mathbf{o} + (u\mathbf{p}_u + v\mathbf{p}_v + \mathbf{p}_t)t \\ &= \mathbf{o} + ut\mathbf{p}_u + vt\mathbf{p}_v + t\mathbf{p}_t. \end{aligned} \quad (3)$$

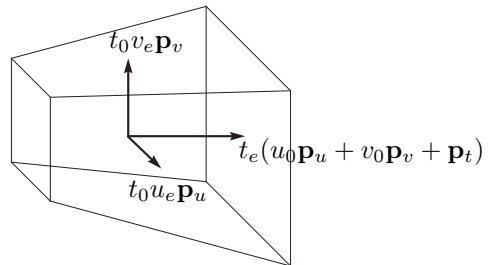


Figure 1: The geometry of a cell. The vectors show the three medial axes of the cell.

The spatial extent of a cell is obtained from the above by having the  $u$ ,  $v$  and  $t$  parameters vary over appropriate intervals  $[u_a, u_b]$ ,  $[v_a, v_b]$  and  $[t_a, t_b]$ . We must consider how to compute the rAA representation  $\hat{\mathbf{x}}$  of this spatial extent. To do so a change of variables must first be performed. The rAA variable  $\hat{u} = u_0 + u_e e_u$  will span the same interval  $[u_a, u_b]$  as  $u$  does if we have:

$$u_0 = (u_b + u_a)/2, \quad (4a)$$

$$u_e = (u_b - u_a)/2. \quad (4b)$$

Similar results apply for the  $v$  and  $t$  parameters. Substituting  $\hat{u}$ ,  $\hat{v}$  and  $\hat{t}$  in (3) for  $u$ ,  $v$  and  $t$ , we get:

$$\begin{aligned} \mathbf{x} = & \mathbf{o} + t_0 u_0 \mathbf{p}_u + t_0 v_0 \mathbf{p}_v + t_0 \mathbf{p}_t \\ & + t_0 u_e e_u \mathbf{p}_u + t_0 v_e e_v \mathbf{p}_v \\ & + u_0 t_e e_t \mathbf{p}_u + v_0 t_e e_t \mathbf{p}_v + t_e e_t \mathbf{p}_t \\ & + t_e u_e e_u e_t \mathbf{p}_u + t_e v_e e_v e_t \mathbf{p}_v. \end{aligned} \quad (5)$$

The first line of (5) contains only constant terms. The second and third lines contain linear terms of the noise symbols  $e_u$ ,  $e_v$  and  $e_t$ . The fourth line contains two non-linear terms  $e_u e_t$  and  $e_v e_t$ , which are a consequence of the non-linearity of the perspective transformation. Since a rAA representation cannot accommodate such non-linear terms they are replaced by the independent noise terms  $e_{k_1}$ ,  $e_{k_2}$  and  $e_{k_3}$  for each of the three cartesian coordinates of  $\hat{\mathbf{x}}$ . The rAA vector  $\hat{\mathbf{x}}$  is finally given by:

$$\begin{aligned} \hat{\mathbf{x}} = & \mathbf{o} + t_0(u_0 \mathbf{p}_u + v_0 \mathbf{p}_v + \mathbf{p}_t) \\ & + t_0 u_e \mathbf{p}_u e_u + t_0 v_e \mathbf{p}_v e_v \\ & + t_e(u_0 \mathbf{p}_u + v_0 \mathbf{p}_v + \mathbf{p}_t) e_t \\ & + [x_{k_1} e_{k_1} \quad x_{k_2} e_{k_2} \quad x_{k_3} e_{k_3}]^T, \end{aligned} \quad (6)$$

with

$$x_{k_i} = |t_e u_e p_{u_i}| + |t_e v_e p_{v_i}|, \quad i = 1, 2, 3. \quad (7)$$

A consequence of the non-linearity of the perspective projection and its subsequent approximation with rAA is that the region spanned by  $\hat{\mathbf{x}}$  is going to be larger than the spatial extent of the cell. Figure 2 shows the geometry of a cell and the region spanned by its rAA representation in profile. Because the rAA representation has been linearised, its spatial extent is a prism rather than a truncated pyramid. This has further consequences in that the evaluation of  $f(\hat{\mathbf{x}})$  is going to include information from the regions of the prism outside the cell and will, therefore, lead to range estimates that are larger than necessary. The linearisation error is more pronounced for cells that exist early in the subdivision process. As subdivision continues and the cells become progressively smaller, their geometry becomes more like that of a prism and the discrepancy with the geometry of  $\hat{\mathbf{x}}$  decreases<sup>2</sup>.

The subdivision of a cell proceeds by first choosing one of the three perspective projection parameters  $u$ ,  $v$  or  $t$  and splitting the cell in half along that parameter. This scheme leads to a  $k$ - $d$  tree of cells where the sequence of dimensional splits is only determined at run time. The choice of which parameter to split along is based on the average width, height and depth

<sup>2</sup>This can be demonstrated by the fact that the terms  $t_e u_e$  and  $t_e v_e$  in (5) decrease more rapidly than any of the linear terms  $u_e$ ,  $v_e$  and  $t_e$  of the same equation as the latter converge to zero.

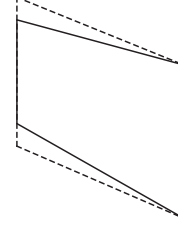


Figure 2: The outline of a cell (solid line) and the outline of its rAA representation (dashed line) shown in profile. The rAA representation is a prism that forms a tight enclosure of the cell.

of the cell:

$$\bar{w}_u = 2 t_0 u_e \|\mathbf{p}_u\|, \quad (8a)$$

$$\bar{w}_v = 2 t_0 v_e \|\mathbf{p}_v\|, \quad (8b)$$

$$\bar{w}_t = 2 t_e \|u_0 \mathbf{p}_u + v_0 \mathbf{p}_v + \mathbf{p}_t\|. \quad (8c)$$

If, say,  $\bar{w}_u$  is the largest of these three measures, the cell is split along the  $u$  parameter. The two child cells will have their  $u$  parameters ranging inside the intervals  $[u_a, u_0]$  and  $[u_0, u_b]$ , where  $[u_a, u_b]$  was the interval spanned by  $u$  in the mother cell. In practice, the factors of 2 in (8) can be ignored without changing the outcome of the subdivision. This subdivision strategy ensures that, after a few iterations, all the cells will have an evenly distributed shape, even when the initial cell is very long and thin.

### 2.3 The Process of Cell Subdivision

Cell subdivision is implemented in an iterative manner rather than using a recursive procedure. The cells are kept sorted in a priority queue based on their level of subdivision. A cell has priority over another if it has undergone less subdivision. For cells at the same subdivision level, the one that is closer to the camera will have priority. The algorithm starts by placing the initial cell, which corresponds to the complete viewing frustum, on the priority queue. At the start of every new iteration, a cell is removed from the head of the queue. If the extent of the cell's projection on the image plane is larger than the extent of a pixel, the cell is subdivided and its two children are examined. In the opposite case, the cell is considered a leaf cell and is discarded after being rendered. The two conditions that indicate whether a cell should be subdivided are:

$$u_b - u_a > 1, \quad (9a)$$

$$v_b - v_a > 1. \quad (9b)$$

The values on the right hand sides of (9) are a consequence of the definition of  $\mathbf{p}_u$  and  $\mathbf{p}_v$  in Section 2.2, which cause all pixels to have a unit width and height.

The sequence of events after a cell has been subdivided depends on which of the parameters  $u$ ,  $v$  or  $t$  was used to perform the subdivision. If the subdivision occurred along  $t$ , there will be two child cells with one in front of the other and totally occluding it. The front cell is first checked for the condition  $0 \in f(\hat{\mathbf{x}})$ . If the condition holds, the cell is pushed into the priority queue and the back cell is ignored. If the condition does not hold, the back cell is also checked for the same condition. The difference now is that, if  $0 \notin f(\hat{\mathbf{x}})$  for the back cell, a new cell must be searched by marching along the  $t$  direction. The first cell scanned, at the same subdivision level of the front and back cells, for which  $0 \in f(\hat{\mathbf{x}})$  holds is the one that is pushed into the priority queue. On the other hand, if the subdivision occurred along the  $u$  or  $v$  directions, there will be two child cells that sit side by side relative to the camera without occluding each other. Both cells are processed in the same way. If, for any of the two cells,  $0 \in f(\hat{\mathbf{x}})$  holds, that cell is placed on the priority queue, otherwise a farther cell must be searched by marching forward in depth.

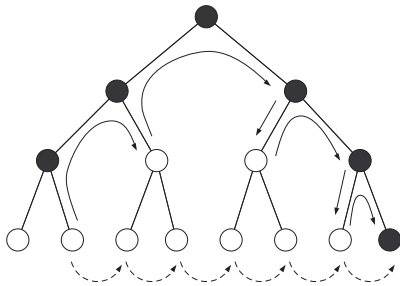


Figure 3: Scanning along the depth subdivision tree. Cells represented by black nodes may intersect with the surface. Cells represented by white nodes do not. The solid arrows show progression by depth-first order. The dotted arrows show progression by breadth-first order.

The process of marching forward from a cell along the depth direction  $t$  tries to find a new cell that has a possibility of intersecting the implicit surface by verifying the condition  $0 \in f(\hat{\mathbf{x}})$ . The process is invoked when the starting cell has been determined not to verify the same condition. The reason for having this scanning in depth is because cells that do not intersect with the surface must be discarded. Only cells that verify  $0 \in f(\hat{\mathbf{x}})$  are allowed into the priority queue for further processing. Figure 3 shows an example of this marching process. The scanning is performed by following a depth-first ordering relative to the tree that results from subdividing in  $t$ . The scanning sequence skips over the children of cells for which  $0 \notin f(\hat{\mathbf{x}})$ . The possibility of scanning in breadth-first order, by marching along all the cells at the same level of subdivision, is not recommended because in deeply subdivided trees a very high number

of cells would have to be tested.

As mentioned before, when subdivision is performed along  $t$ , the back cell is ignored whenever the front cell verifies  $0 \in f(\hat{\mathbf{x}})$ . This does not mean, however, that the volume occupied by this back cell will be totally discarded from further consideration. The front cell may happen to be subdivided during subsequent iterations of the algorithm and portions of the volume occupied by the back cell may then be revisited by the depth marching procedure.

## 2.4 Rendering a Cell

The shading value of a cell is obtained by evaluating the shading function at the centre of the cell. The central point  $\mathbf{x}_0$  for the cell is determined from (6) to be:

$$\mathbf{x}_0 = \mathbf{o} + t_0(u_0\mathbf{p}_u + v_0\mathbf{p}_v + \mathbf{p}_t). \quad (10)$$

During rendering, the shading value of a cell is assigned to all the pixels that are contained within its image plane projection. The centre of a pixel  $(i, j)$  occupies the coordinates  $\mathbf{c}_{ij} = (i + 1/2, j + 1/2)$  on the image plane. All the pixels that verify  $\mathbf{c}_{ij} \in [u_a, u_b] \times [v_a, v_b]$  for the cell being rendered will be assigned its shading value. Any previous shading values stored in these pixels will be overwritten. This process happens after cell subdivision and before the newly subdivided cells are placed on the priority queue. The subdivided cells will overwrite the shading value of their mother cell on the image buffer. The same process also takes place for leaf cells before they are discarded. In this way, the image buffer always contains the best possible representation of the image at the start of every new iteration.

## 2.5 Specifying a Region of Interest

A user can interactively influence the rendering algorithm by drawing a rectangular region of interest (ROI) over the image. The algorithm will then refine the image only inside the specified region. This is accomplished by creating a secondary priority queue that stores the cells that are relevant to the ROI. When the user finishes drawing the region, the primary queue is scanned and all cells whose image projection intersects with the rectangle corresponding to that ROI are transferred to the secondary queue. The algorithm then proceeds as explained in Section 2.3 with the difference that the secondary queue is now being used. Once this queue becomes empty, the portion of the image inside the ROI is fully rendered and the algorithm returns to subdividing the cells that were left in the primary queue. It is also possible to cancel the ROI at any time by flushing any cells still in the secondary queue back to the primary queue.

## 2.6 Some Implementation Remarks

The best implementation strategy for our rendering method is to have an application that runs two threads concurrently: a subdivision thread and a rendering thread. The rendering thread is responsible for periodically updating the graphical output of the application with the latest results from the subdivision thread. A timer is used to keep a constant frame refresh rate. Except for the periodical invocation of the timer handler routine, the rendering thread remains in a sleep state so that the subdivision thread can use all the CPU resources.

## 3 RESULTS

Figure 5 at the end of the paper shows four snapshots taken during the progressive refinement rendering of an implicit sphere modulated with a Perlin procedural noise function (Perlin, 2002). The last snapshot shows the final rendering of the surface. The large scale features of the surface become settled quite early and the latter stages of the refinement are mostly concerned with resolving small scale details.

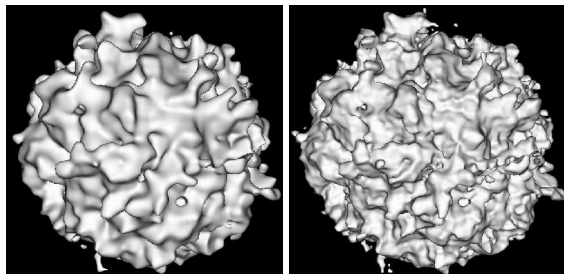


Figure 4: An implicit surface with two layers (left) and three layers (right) of a Perlin noise function.

Figure 4 shows an implicit sphere modulated with two and three layers of the Perlin noise function. Table 1 shows the total number of iterations and the computation time for the surfaces that were rendered in Figures 4 and 5. The table also shows the computation time for ray casting the same surfaces by shooting a single ray through the centre of each pixel. The results in Table 1 were obtained on a laptop with a Pentium 4 1.8 GHz processor and 1 Gbyte of memory. The number of iterations required to complete the progressive rendering algorithm is largely independent of the complexity of each surface. It depends only on the image resolution and on the percentage of the image that is covered by the projected surface.

As estimated by the results in Table 1, previewing by progressive refinement is approximately three times faster than previewing by ray casting without

<i>Layers</i>	<i>Iterations</i>	<i>Time</i>	<i>Raycasting</i>
1	350759	27.8s	1m10.4s
2	349465	1m16.8s	4m16.7s
3	359659	3m01.5s	8m51.7s

Table 1: Rendering statistics for an implicit sphere with several layers of Perlin noise.

anti-aliasing. It should be added that these numbers do not entirely reflect the reality of the situation because, as demonstrated in the example of Figure 5, progressive refinement previewing already gives an accurate rendering of the surface at early stages of refinement. From a perceptual point of view, therefore, the difference between the two previewing techniques is greater than what is shown in Table 1.

Figure 6 shows two snapshots of a progressive refinement rendering where a region of interest is active. The surface being rendered is the same two layer Perlin noise surface that was shown in Figure 4. The rectangular ROI is defined on the lower right corner of the image. The portion of the surface that projects inside the ROI is given priority during progressive refinement.

## 4 CONCLUSIONS

The rendering method, here presented, offers the possibility of visualising implicit surfaces with progressive refinement. The main features of a surface become visible early in the rendering process, which makes this method ideal as a previewing tool during the editing stages of an implicit surface modeler. In comparison, a meshing method would generate expensive high resolution preview meshes for the more complex surfaces while a ray caster would be slower and without the progressive refinement feature. Our rendering method, however, does not implement anti-aliasing and cannot compete with an anti-aliased ray caster as a production tool. Production quality renderings of some of the surfaces shown in this paper are typically done overnight, a fact which further justifies the need for a previewing tool.

It would have been straightforward to incorporate anti-aliasing into our rendering method by allowing cells to be subdivided down to sub-pixel size and then applying a low-pass filter to reconstruct the pixel samples. There is, however, one issue that prevents the use of our method as a production tool and which makes this implementation effort not worth the while. As explained in Section 2.1, the computation of range estimates with affine arithmetic is always conservative. This conservativeness implies that some cells a small distance away from the surface may be incorrectly flagged as intersecting with it. As a con-

sequence, some portions of the surface may appear dilated after rendering. The surface offset error is in the same order as the size of a pixel. This artifact can be tolerated during previewing but is not acceptable for production quality renderings.

We intend in the future to apply our progressive refinement previewing strategy not only to procedural fractal planets in implicit form but also to implicit surfaces that interpolate scattered data points.

## REFERENCES

- Bergman, L., Fuchs, H., Grant, E., and Spach, S. (1986). Image rendering by adaptive refinement. In Evans, D. C. and Athay, R. J., editors, *Computer Graphics (SIGGRAPH '86 Proceedings)*, pages 29–37.
- Bloomenthal, J. (1988). Polygonisation of implicit surfaces. *Computer Aided Geometric Design*, 5:341–355.
- Cohen, M. F., Chen, S. E., Wallace, J. R., and Greenberg, D. P. (1988). A progressive refinement approach to fast radiosity image generation. In Dill, J., editor, *Computer Graphics (SIGGRAPH '88 Proceedings)*, pages 75–84.
- Comba, J. L. D. and Stolfi, J. (1993). Affine arithmetic and its applications to computer graphics. In *Proc. VI Brazilian Symposium on Computer Graphics and Image Processing (SIBGRAP '93)*, pages 9–18.
- Cook, R. L. (1989). Stochastic sampling and distributed ray tracing. In Glassner, A. S., editor, *An Introduction to Ray Tracing*, chapter 5, pages 161–199. Academic Press.
- de Figueiredo, L. H. (1996). Surface intersection using affine arithmetic. In Davis, W. A. and Bartels, R., editors, *Graphics Interface (GI '96)*, pages 168–175.
- de Figueiredo, L. H. and Stolfi, J. (1996). Adaptive enumeration of implicit surfaces with affine arithmetic. *Computer Graphics Forum*, 15(5):287–296.
- de Figueiredo, L. H., Stolfi, J., and Velho, L. (2003). Approximating parametric curves with strip trees using affine arithmetic. *Computer Graphics Forum*, 22(2):171–171.
- Desbrun, M. and Gascuel, M. (1995). Animating soft substances with implicit surfaces. In Cook, R., editor, *Computer Graphics (SIGGRAPH '95 Proceedings)*, pages 287–290.
- Ebert, D. S., Musgrave, F. K., Peachey, D., Perlin, K., and Worley, S. (2003). *Texturing & Modeling: A Procedural Approach*. Morgan Kaufmann Publishers Inc., third edition.
- Farrugia, J. P. and Peroche, B. (2004). A progressive rendering algorithm using an adaptive perceptually based image metric. *Computer Graphics Forum*, 23(3):605–614.
- Foster, N. and Fedkiw, R. (2001). Practical animation of liquids. In Pockock, L., editor, *Computer Graphics (SIGGRAPH '01 Proceedings)*, pages 23–30.
- Guo, B. (1998). Progressive radiance evaluation using directional coherence maps. In Cohen, M., editor, *Computer Graphics (ACM SIGGRAPH '98 Proceedings)*, pages 255–266.
- Heidrich, W. and Seidel, H.-P. (1998). Ray-tracing procedural displacement shaders. In Davis, W., Booth, K., and Fournier, A., editors, *Graphics Interface (GI '98)*, pages 8–16.
- Heidrich, W., Slusallik, P., and Seidel, H. (1998). Sampling procedural shaders using affine arithmetic. *ACM Transactions on Graphics*, 17(3):158–176.
- Hin, A. J. S., Boender, E., and Post, F. H. (1989). Visualization of 3D scalar fields using ray casting. In *Eurographics Workshop on Visualization in Scientific Computing*.
- Junior, A., de Figueiredo, L., and Gattas, M. (1999). Interval methods for raycasting implicit surfaces with affine arithmetic. In *Proc. XII Brazilian Symposium on Computer Graphics and Image Processing (SIBGRAP '99)*, pages 1–7.
- Kolb, C. E. (1992). Rayshade user's guide and reference manual. Draft 0.4.
- Laur, D. and Hanrahan, P. (1991). Hierarchical splatting: A progressive refinement algorithm for volume rendering. In Sederberg, T. W., editor, *Computer Graphics (SIGGRAPH '91 Proceedings)*, pages 285–288.
- Lippert, L. and Gross, M. H. (1995). Fast wavelet based volume rendering by accumulation of transparent texture maps. *Computer Graphics Forum*, 14(3):431–444.
- Lorensen, W. E. and Cline, H. E. (1987). Marching cubes: A high resolution 3D surface construction algorithm. In Stone, M. C., editor, *Computer Graphics (SIGGRAPH '87 Proceedings)*, pages 163–169.
- Messine, F. (2002). Extensions to affine arithmetic: Application to unconstrained global optimization. *Journal of Universal Computer Science*, 8(11):992–1015.
- Mitchell, D. P. (1990). Robust ray intersection with interval arithmetic. In MacKay, S. and Kidd, E. M., editors, *Graphics Interface (GI '90)*, pages 68–74.
- Moore, R. (1966). *Interval Arithmetic*. Prentice-Hall, Englewood Cliffs (NJ), USA.
- Perlin, K. (2002). Improving noise. *ACM Transactions on Graphics*, 21(3):681–682.
- Roth, S. D. (1982). Ray casting for modeling solids. *Computer Graphics and Image Processing*, 18(2):109–144.
- Velho, L. (1996). Simple and efficient polygonization of implicit surfaces. *Journal of Graphics Tools*, 1(2):5–24.
- Whitaker, R. T. (1998). A level-set approach to 3D reconstruction from range data. *Int. J. Computer Vision*, 29:203–231.

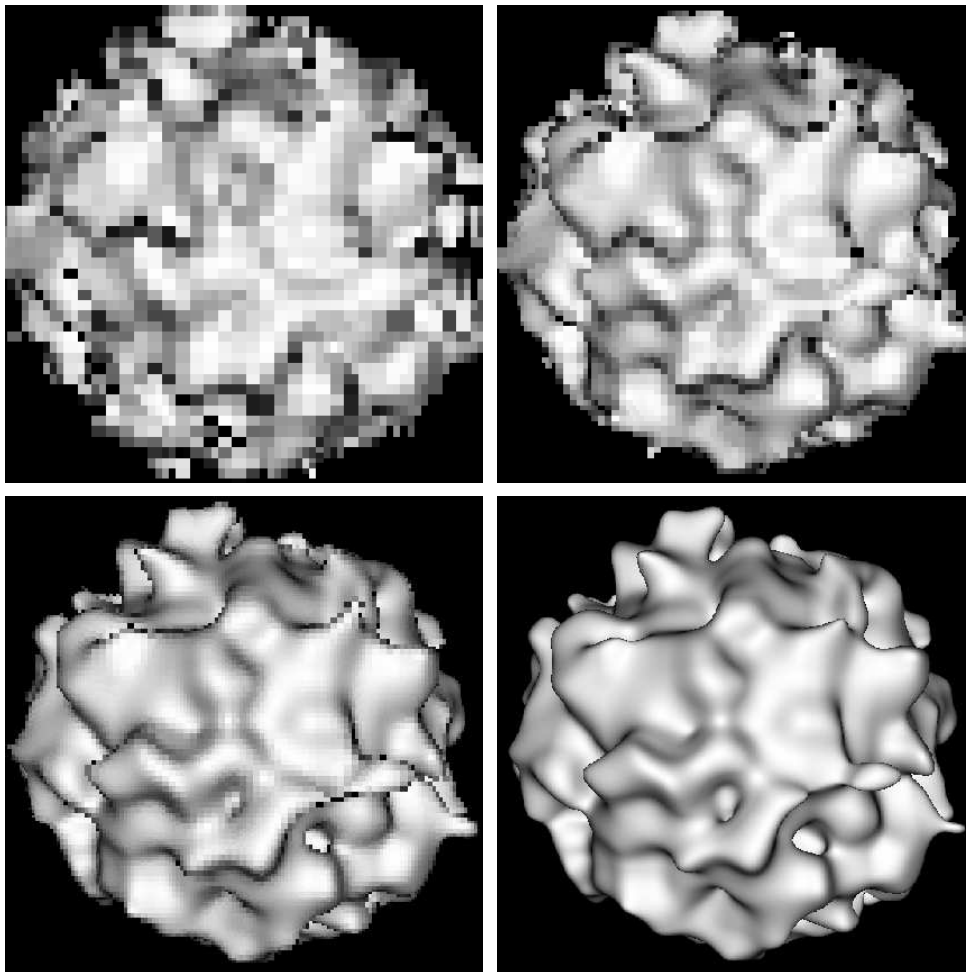


Figure 5: From left to right, top to bottom, snapshots taken during the progressive refinement rendering of a procedural noise function. The snapshots were taken after 5000, 10000, 28000 and 350759 iterations, respectively. The wall clock times at each snapshot are 1.02s, 1.98s, 4.18s and 27.80s, respectively.

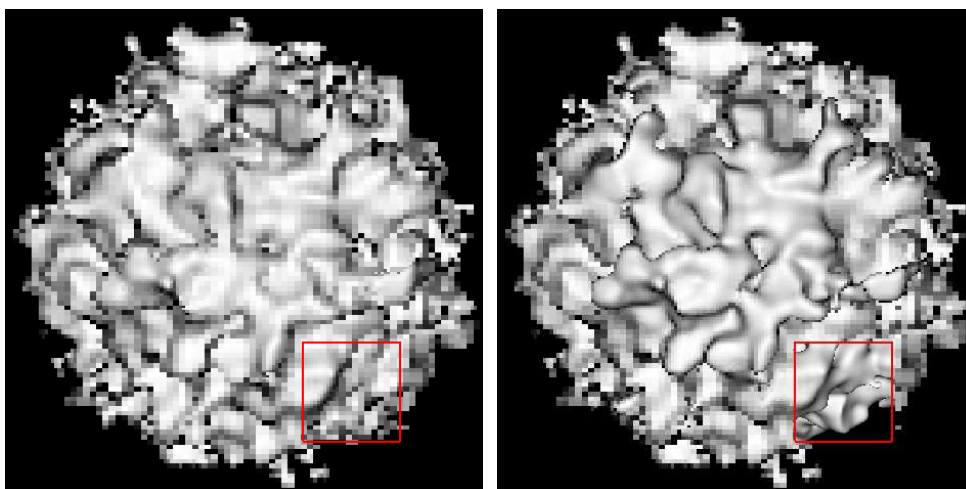


Figure 6: Progressive refinement rendering with an active region of interest shown as a red frame. Once rendering is complete inside the region, refinement continues on the rest of the image.